Journal of ELECTRONIC MATERIALS
DOI: 10.1007/s11664-016-4650-y

A Novel Route for Preparing Highly Stable Fe_3O_4 Fluid with Poly(Acrylic Acid) as Phase Transfer Ligand

VUONG THI KIM OANH,[1] TRAN DAI LAM,[2,3,7,8] VU THI THU,[4] LE TRONG LU,[5] PHAM HONG NAM,[1] LE THE TAM,[6] DO HUNG MANH,[1] and NGUYEN XUAN PHUC[1,9]

1.—Institute of Materials Science, Vietnam Academy of Science and Technology, 18 Hoang Quoc Viet Road, Hanoi, Vietnam. 2.—Graduate University of Science and Technology, Vietnam Academy of Science and Technology, 18 Hoang Quoc Viet Road, Hanoi, Vietnam. 3.—Duy Tan University, 182 Nguyen Van Linh, Danang, Vietnam. 4.—University of Science and Technology of Hanoi, 18 Hoang Quoc Viet Road, Hanoi, Vietnam. 5.—Institute for Tropical Technology, Vietnam Academy of Science and Technology, 18 Hoang Quoc Viet Road, Hanoi, Vietnam. 6.—Vinh University, 182 Le Duan, Vinh, Vietnam. 7.—e-mail: tdlam@gust-edu.vast.vn, 8.—e-mail: trandailam@gmail.com, 9.—e-mail: phucnx@ims.vast.ac.vn

Highly stable Fe_3O_4 liquid was synthesized by thermal decomposition using poly(acrylic acid) (PAA) as a phase transfer ligand. The crystalline structure, morphology, and magnetic properties of the as-prepared samples were thoroughly characterized. Results demonstrated that the magnetic Fe_3O_4 nanomaterial was formed in liquid phase with a spinel single-phase structure, average size of 8–13 nm, and high saturation magnetization (up to 75 emu/g). The PAA-capped Fe_3O_4 nanoparticles displayed high stability over a wide pH range (from 4 to 7) in 300 mM salt solution. More importantly, the heat-generating capacity of the nanoparticle systems was quantified at a specific absorption rate (SAR) of 70.22 W/g, which is 35% higher than magnetic nanoparticles coated with sodium dodecyl sulfate (SDS). These findings suggest the potential application of PAA-coated magnetic nanoparticles in magnetic hyperthermia.

Key words: Hyperthermia, nanostructures, magnetic liquid, poly(acrylic acid), ligand exchange

INTRODUCTION

Magnetic nanoparticles have been widely used in various fields including information technology, environmental treatments, catalysis, and biomedical applications.[1–4] In several of these applications—for instance, hyperthermia treatment of cancer—it is beneficial to have magnetic nanoparticles with uniform small size (D ca. 10 nm), good dispersion, high stability, and high saturation magnetization ($M_S > 70$ emu/g), so that they can respond sensitively to a small external magnetic field or enhance the efficiency of magnetic induction heating.[5,6] Among these magnetic nanomaterials, Fe_3O_4 is most favored for biomedical applications, thanks to its biocompatibility and facile synthesis.

Many methods have been proposed for the synthesis of Fe_3O_4 nanoparticles, including co-precipitation, sol–gel, and hydrothermal and thermal decomposition techniques.[7,8] Thermal decomposition is among the most widely used methods, given its ability to generate uniform particles with high saturation magnetization.[9,10] In our previous work,[11] Fe_3O_4 fluid was prepared by thermal decomposition using sodium dodecyl sulphate (SDS) as phase transfer agent. The magnetic heating study of that system demonstrated its relatively high specific absorption rate (SAR), but this value was not stable over time. Recently reported works have noted that the stability of magnetic fluid might be improved by coating magnetic particles with an organic layer.[12–15] The presence of such a layer may

(Received January 23, 2016; accepted May 11, 2016)

Published online: 26 May 2016

create a core–shell interaction between the magnetic core and organic shell to maintain the stability of the magnetic fluid while at the same time enhancing its magnetic properties. For instance, magnetic properties can be enhanced by hydrophilic ligands carrying dopamine (DPA) with strong bonds between two –OH groups of DPA molecule and the surface of magnetic nanoparticles.[16] In this paper, we describe a new, convenient thermal decomposition-based approach for the synthesis of Fe_3O_4 liquid using poly(acrylic acid) as the phase transfer ligand. This hydrophilic coating should improve the stability of magnetic nanoparticles in aqueous solution. In addition, this organic coating layer may give rise to enhanced magnetic behaviors and heating magnetic induction of magnetic nanoparticles.

EXPERIMENTAL

Chemicals

Iron (III) acetylacetonate ($Fe(acac)_3$), oleylamine (OLA), oleic acid (OA), poly(acrylic acid) (PAA), and triethylene glycol (TEG) were purchased from Sigma-Aldrich.

Synthesis of Fe_3O_4

The protocol for the synthesis of magnetic nanoparticles was described in our previous work.[11] Briefly, $Fe(acac)_3$ (4 mmol), oleic acid (20 mmol), and oleylamine (20 mmol) were placed in a flask containing 40 ml of dibenzyl ether. This mixture was then stirred for 30 min, before heating to different reaction temperatures (265°C, 285°C, 298°C) over the same reaction time of 2 h. The obtained solutions were then cooled naturally to room temperature, washed with ethanol, and centrifuged, after which they were dispersed in *n*-hexane. They were then dried and denoted as M1, M2, and M3, corresponding to the increasing reaction temperatures.

Synthesis of Fe_3O_4 Magnetic Fluid

Two grams of PAA was dissolved in 40 ml TEG solution, and the mixture was heated to 110°C, at which point 5 ml *n*-hexane solution containing 100-mg magnetic nanoparticles was quickly added to the reaction mixture. The reaction temperature was increased to 280°C and was then kept constant for 6 h.

After completion of the reaction, the obtained product was cooled to room temperature. The PAA-capped magnetic nanoparticles were separated from TEG by adding an excess amount of diluted hydrochloric acid solution. The nanoparticles were then precipitated by centrifugation. After removing the supernatant, the residue was dispersed in water using ultrasound. These magnetic fluids were labeled L1, L2, and L3, correspondingly, for M1, M2, and M3. Figure 1 represents the transformation of the magnetic nanoparticles from a non-aqueous to aqueous phase.

Characterization of Magnetic Nanoparticles

X-ray Diffraction and Fourier Transform Infrared (FT-IR) Spectroscopy

The crystal structure of the samples before and after coating with PAA was determined using the Siemens D5000 diffractometer with Cu-Kα radiation (λ = 1.5406 Å) at room temperature. The average crystal size was acquired with X'Pert HighScore Plus commercial image analysis software. The shell–core bonds were analyzed by Fourier transform infrared spectroscopy (FT-IR; Nicolet 6700).

Transmission Electron Microscopy (TEM)

The morphological properties (size and shape) of the particles were obtained using transmission electron microscopy (TEM; JEOL JEM-1010).

Vibrating Sample Magnetometer (VSM)

The saturation magnetization of the samples at room temperature was measured under the highest magnetic field of 10 kOe using a vibrating sample magnetometer (VSM) (home-made).

Size Measurement

The size distribution and stability of the magnetic fluids were examined using the Zetasizer (Nano ZS-Malvern-UK).

Magnetic Induction Heating

The effect of magnetic induction heating on the magnetic fluid was determine based on the Fe_3O_4 nanoparticles with the highest saturation magnetization and uniform particle size (sample L3) under an alternating magnetic field in a range of 50–80 Oe and frequency of f = 178 kHz, provided by the commercial generator (RDO HFI 5KW).

RESULTS AND DISCUSSION

Morphology and Particle Size

The morphology and particle size of the magnetic nanoparticles before and after phase transfer were evaluated by TEM, and TEM images of the transferred magnetic nanoparticles are presented in Fig. 2.

As is evident in Fig. 2, the magnetic particles were well dispersed in liquid form, with relatively narrow size distribution. Here, the use of a coating material with a hydrophilic nature, such as PAA, helped to improve the dispersion of the magnetic nanoparticles in aqueous phase,[11] a feature that is extremely important for biomedical applications of magnetic particles.

In addition, the size of the magnetic particles was almost the same before and after phase transfer, as

A Novel Route for Preparing Highly Stable Fe_3O_4 Fluid with Poly(Acrylic Acid) as Phase Transfer Ligand

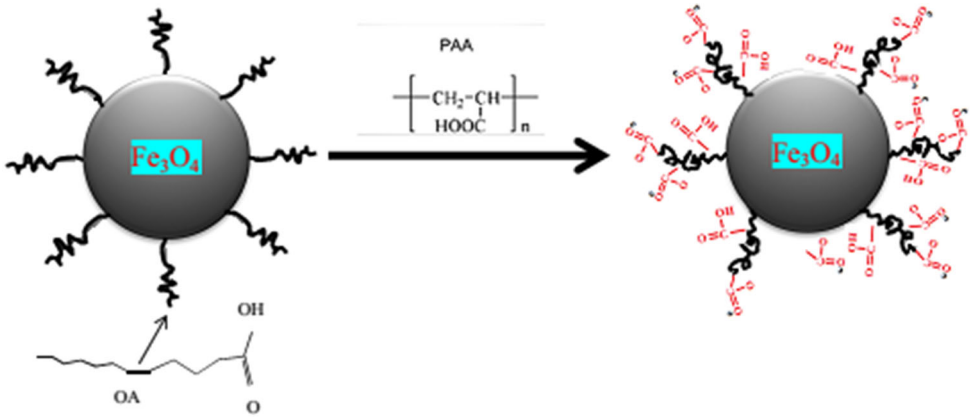

Fig. 1. Schematic of the ligand exchange process using PAA.

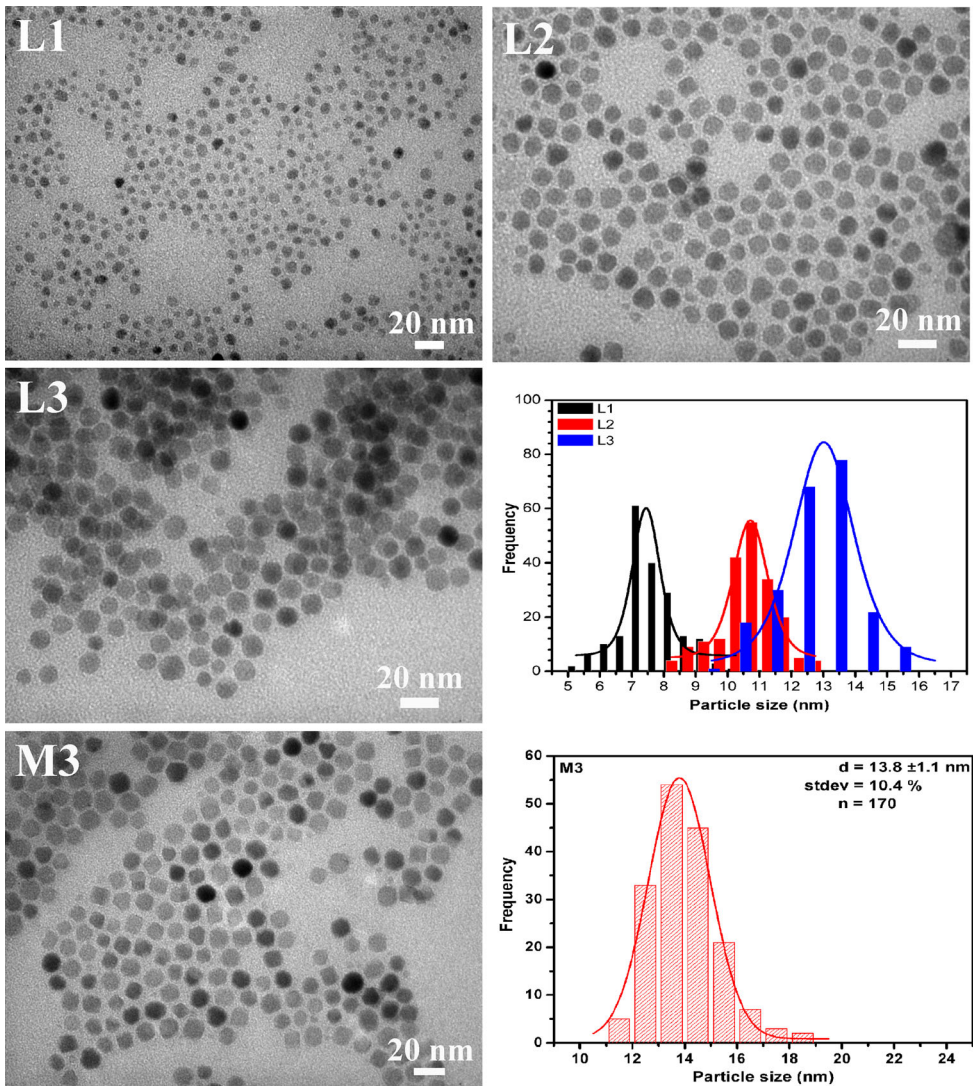

Fig. 2. TEM images and particle size distribution of post-transfer samples (L1, L2, L3) and a pre-transfer sample (M3).

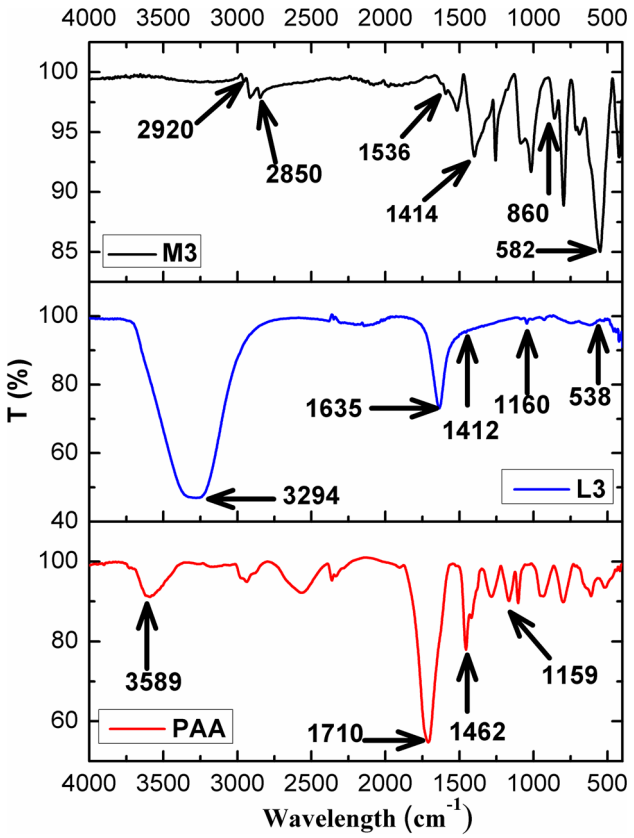

Fig. 3. FT-IR spectra of L3, poly(acrylic acid) (PAA) and M3 samples.

the synthesized outer layer was quite efficiently exchanged by the transferring PAA material.

FT-IR

FT-IR spectroscopy was performed to confirm the interaction between PAA and iron oxide nanoparticles (Fig. 3). The samples were washed several times with water to remove free molecules before characterization.

The characteristic vibration of Fe–O bonding was clearly observed on FT-IR spectra at 538/cm (Fig. 3). The FT-IR spectrum of sample L3 also showed vibration peaks at 1635 and 1160/cm, assigned to C=O and C–O–C in PAA molecules. The positions of these peaks compared to the bare PAA sample were shifted toward a longer wavelength, since the PAA molecules were no longer free, but were deposited on the surface of the magnetic particles. The occurrence of vibration peaks characteristic of the carboxyl group (1412/cm) on the FT-IR spectrum again confirmed the presence of the PAA coating layer.[11,17,18]

Magnetic Properties

Figure 4a presents the hysteresis loops of the three samples L1, L2, and L3 at room temperature, from which it is evident that the phase transfer played an important role in enhancing the magnetization of the samples, by approximately 5% (compared with pre-transfer samples in Fig. 4b). The improvement in the magnetic properties of the magnetite particles is clearly due to the action of organic functional groups (i.e., COOH, OH, etc.) on the outer layer. These ligands have somehow oriented the magnetic domains near the surface of particles toward the same direction as magnetic moment of the magnetite core.[16]

The $M(H)$ curves of the samples were also analyzed using the Langevin theory, as described in our previous work.[11]

With small magnetic nanoparticles, it is difficult to observe magnetic saturation with an external magnetic field of 10 kOe. This may be associated with the particle size effect, in which small particles need a larger magnetic field in order to reverse the spins at the particle boundaries toward the direction of the external magnetic field. Therefore, to determine the true M_S, we used an extrapolation according to the 'Law of approach to saturation' (LAS)[19] as expressed in the equation:

$$M(H) = M_S\left[1 - \frac{a}{H} - \frac{b}{H^2}\right] + \chi_d H,$$

where M_S is the saturation magnetization and χ_d is the high-field differential susceptibility.

The results are shown in Fig. 4c and Table I. The magnetization of the magnetic nanoparticles in pre-transfer (sample M3) and post-transfer phases (sample L3) was 70 emu/g and 75 emu/g, respectively. This slight increase in magnetization of magnetite particles is assumed to reflect the variation in the nature of the outer coating layer.

Compared to those in previously reported works, the aqueous magnetic particles prepared using our approach showed better magnetic properties. For example, the magnetization of magnetic nanoparticles with a poly(styrene-co-acrylic acid) shell prepared by co-precipitation was only 70 emu/g, even with larger-sized particles.[20]

Stability

The stability of particles in a physiological environment is essential in biomedical applications. Thus, the hydrophilic exteriors of these particles must be designed to be stable in aqueous solutions within a certain range of pH and salt concentration. Here, the dispersion of magnetic nanoparticles in an aqueous environment was tested at pH 5–9 and NaCl salt concentrations of 100–300 mM. The sample prepared at a high temperature (298°C) with the narrowest size distribution and highest saturated magnetization was chosen for this experiment.

Figure 5 shows optical images of magnetic nanoparticles dispersed in aqueous solutions at different salt concentrations and pH. The PAA-capped magnetic nanoparticles are visibly well-

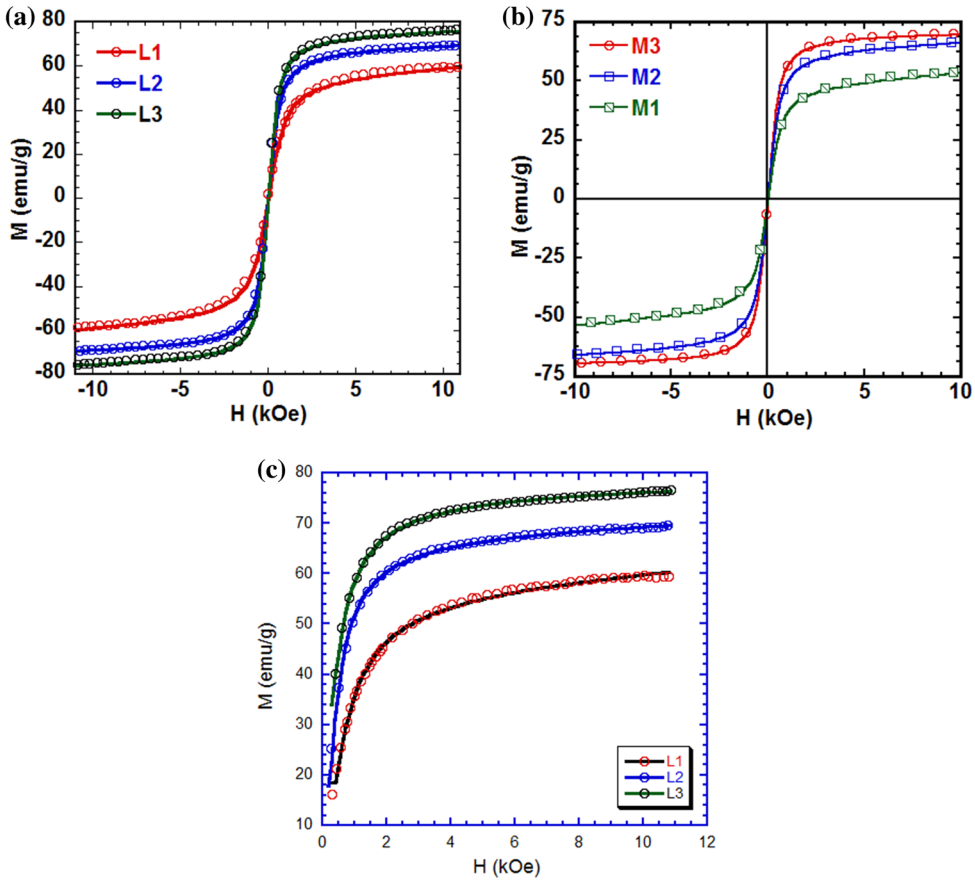

Fig. 4. $M(H)$ curves of (a) post-transfer samples (L1, L2, L3), (b) pre-transfer samples (M1, M2, M3), and (c) fitted by the LAS method. The symbols show measured data. The solid lines show the fit of the Langevin function or LAS method.

Table I. Average nanoparticle size (D_{TEM}) and saturation magnetization determined from measured $M(H)$ curves (M_S^*) and from the LAS method (M_S)

Sample	D_{TEM} (nm)	M_S^* (emu/g)	M_S (emu/g)
L1	8	58	60.9
L2	11	69	69.1
L3	13	75	77.2

dispersed in a physiological environment (salt concentration = 100–300 mM and pH = 5–7). Such high stability of ferrofluid under physiological conditions renders it suitable for many biomedical applications. At higher salt concentrations and lower pH, the magnetic particles were aggregated and formed visible precipitate at the bottom of the flask. As evidenced by zeta analysis, the particle size was increased tenfold with an increase in salt concentration to more than 500 mM or a decrease in pH to 3 (Fig. 6).

Magnetic Induction Heating

The highly stable sample (L3) was used to further investigate the magnetic heating effect. The maximum temperature (T_{max}) and the specific absorption rate (SAR) of the samples were determined at different sample concentrations and different magnetic field amplitudes.

The SAR is defined as the variation in temperature with time ($\Delta T/\Delta t$) of the ferrofluid in the ac magnetic field, as follows:

$$\mathrm{SAR} = C\frac{m_{\mathrm{sample}}}{m_{\mathrm{mnp}}}\left(\frac{\Delta T}{\Delta t}\right),$$

where C is the specific heat of the fluid per mass unit (C = 4.18 J/gK), m_{sample}/m_{mnp} is the nanoparticle concentration in the fluid (with m_{sample} = 1000 mg; m_{mnp} = 1,2, 3,4, 5 mg), and $\Delta T/\Delta t$ is the initial slope of the heating curves.

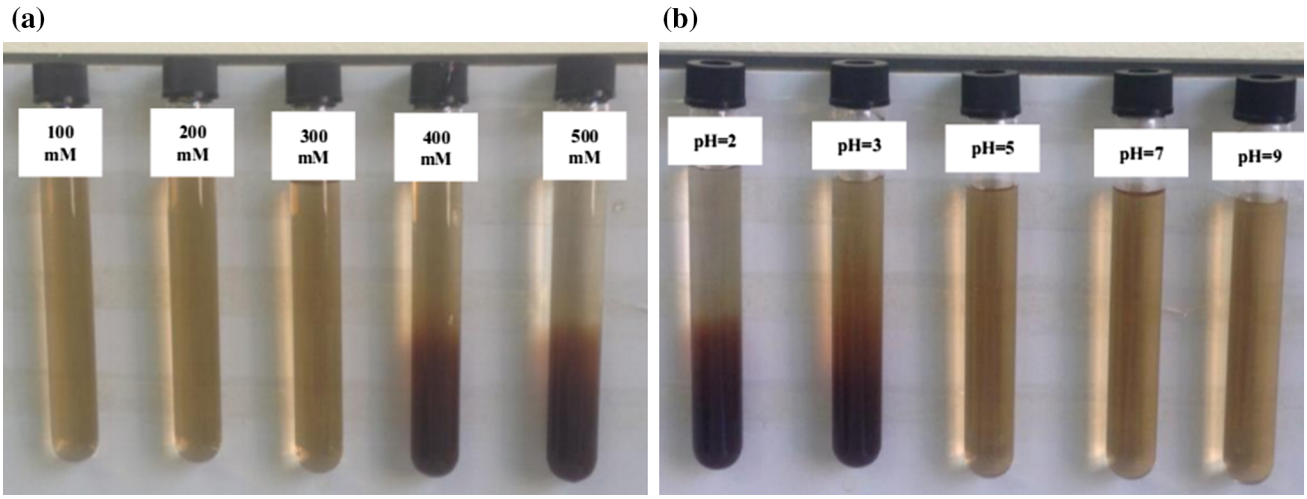

Fig. 5. Photo images of the L3 sample at different salt concentrations (a) and pH (b).

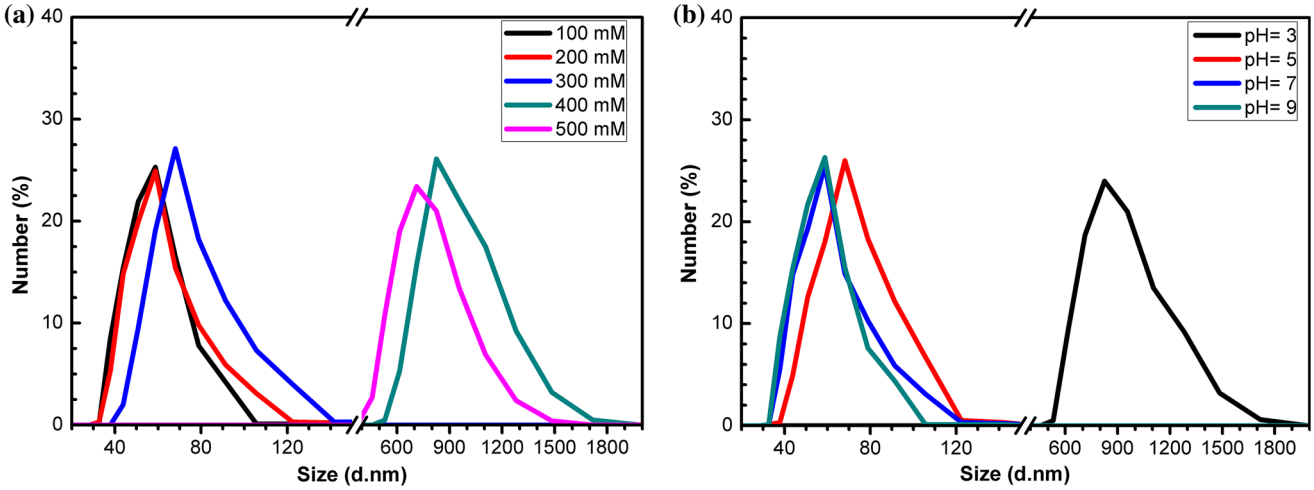

Fig. 6. The particle size distribution patterns of L3 at different salt concentrations (a) and pH (b).

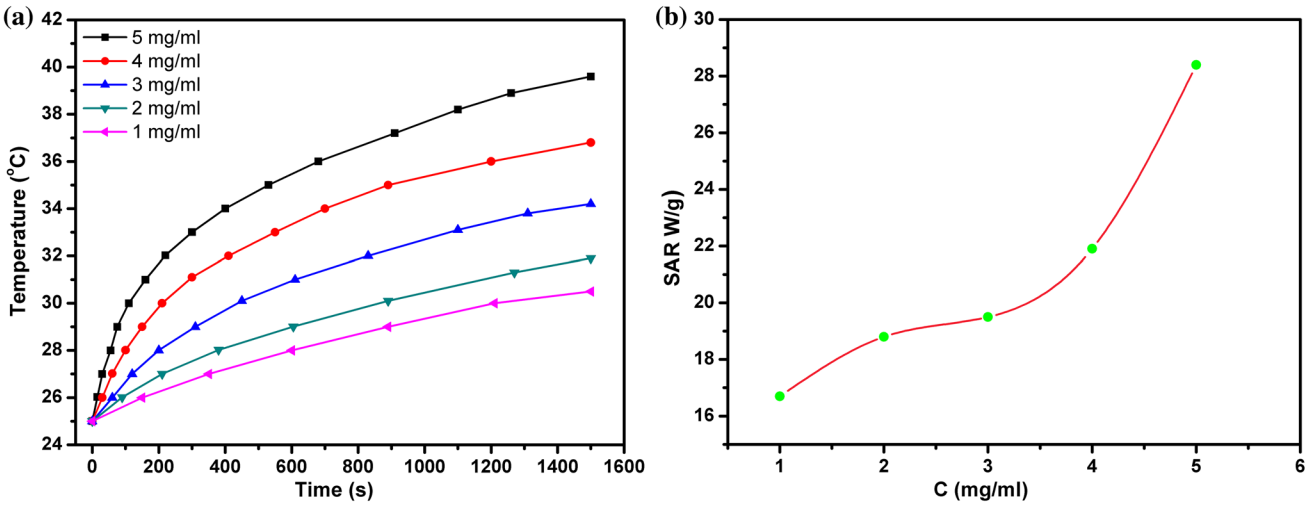

Fig. 7. Heating induction effect for the L3 sample. (a) Magnetic heating curves measured for suspensions of the L3 sample at different particle concentrations; (b) SAR determined at different particle concentrations of the L3 sample. Magnetic field amplitude is 50 Oe. Magnetic frequency is 178 kHz.

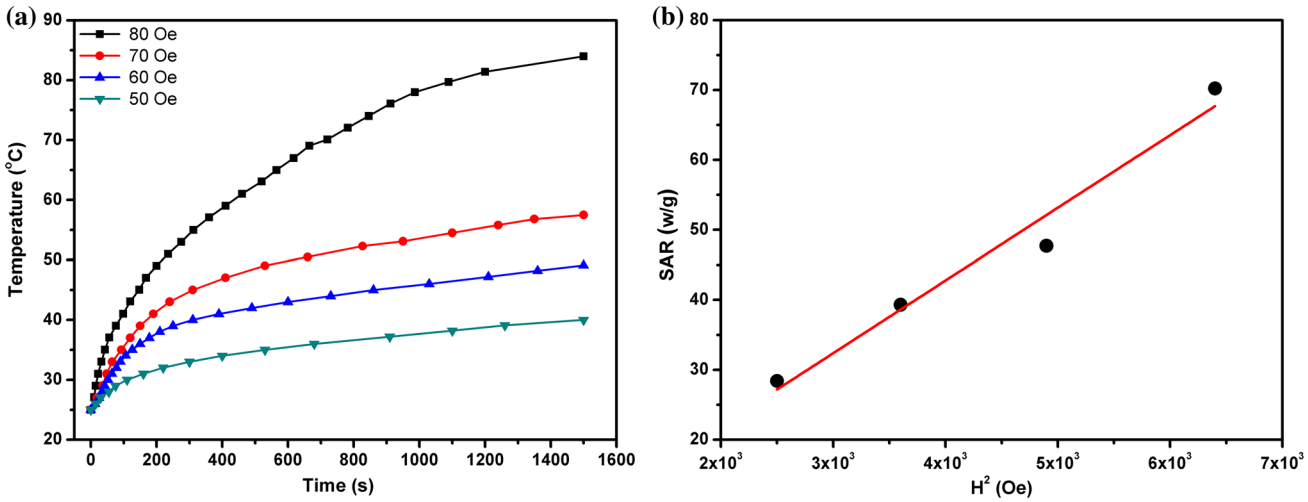

Fig. 8. Magnetic heating curves measured for suspensions of samples (L3) at 5 mg/ml at different values of magnetic field strength (a) and the specific absorption rate (SAR) versus magnetic field strength (H^2) square (b).

Table II. Maximum temperature ($T_{1500\ s}$), specific absorption rate (SAR), and initial heating rate ($\Delta T/\Delta t$) of the (L3) ferrofluid sample at 5 mg/ml concentration at different magnetic field strength values

Sample	Magnetic field (H [Oe], f [kHz])	$T_{1500\ s}$	SAR (W/g)	$\Delta T/\Delta t$ (°C/s)
L3 (5 mg/ml)	50, 178	39.6	28.4	0.034
	60, 178	49.1	39.3	0.047
	70, 178	57.5	47.7	0.057
	80, 178	84.1	70.22	0.084

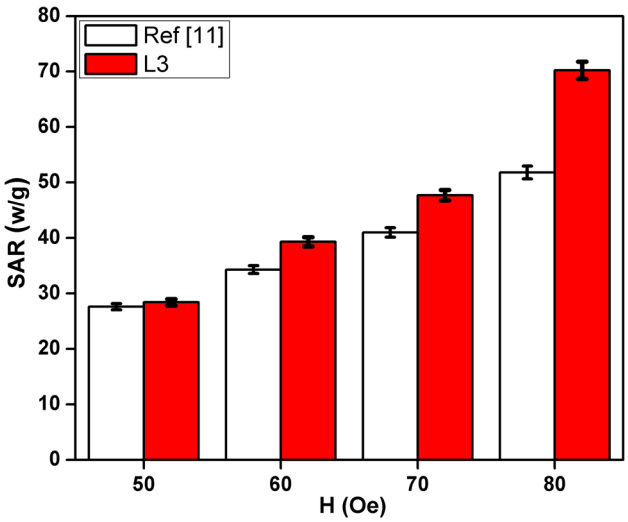

Fig. 9. Comparison of the specific absorption rate of Fe_3O_4 magnetic nanoparticles coated with SDS[11] and coated with poly(acrylic acid) at different magnetic fields.

Figure 7 illustrates the magnetic heating curves of ferrofluids at different concentrations (1–5 mg/ml). The amplitude and frequency of the external magnetic field were 50 Oe and 178 kHz, respectively. As can be seen in Fig. 7, the increase in ferrofluid concentration resulted in a slightly improved magnetic heating effect. The maximum temperature reached 39.6°C, and the SAR was only 28.4 W/g at a particle concentration of 5 mg/ml. This weak heating induction is not sufficient for biomedical applications of magnetic fluid in MRI and hyperthermia treatment.

Figure 8 represents magnetic heating curves measured at different magnetic field strengths. The ferrofluid concentration was 5 mg/ml and the magnetic field frequency was 178 kHz. Unlike the ferrofluid concentration, the amplitude of the magnetic field strongly affected the magnetic heating behaviors of the material. Both the maximum temperature and SAR increased sharply with increasing magnetic field amplitude (Table II).

Compared to Fe_3O_4 nanoparticles coated with SDS in our previous work,[11] the magnetic particles with a PAA shell showed much better magnetic heating induction (Fig. 9). The SAR value was increased 35% by changing the outer shell from SDS to PAA. A relatively high temperature of 70.22°C was obtained at a magnetic field amplitude of 80 Oe.

Table III. Comparison of specific absorption rate (SAR) and intrinsic loss power (ILP)

Parameters	Current study	Ref. 11	Ref. 20
D_{TEM}	13 nm	13 nm	15 nm
AC field parameters	H = 6.4 kA/m, f = 178 kHz	H = 6.4 kA/m, f = 178 kHz	H = 12 kA/m, f = 300 kHz
Concentration	5 mg/ml	5 mg/ml	15 mg/ml
SAR (W/g)	70.22	51.8	86.87
ILP (nHm^2/kg)	9.6	7.1	2.03

The PAA molecules (1800 g/mol) are able to bind strongly to the surface of magnetic nanoparticles thanks to their carboxyl groups. Here, we demonstrated that Fe_3O_4 nanoparticles capped with PAA molecules showed better dispersion and higher stability in aqueous solutions, whereas Fe_3O_4 modified with SDS is unstable and can be easily precipitated. In addition, the PAA coating appeared to increase the saturated magnetization. For these reasons, Fe_3O_4/PAA exhibited better magnetic heating induction compared to Fe_3O_4/SDS.

The intrinsic loss power (ILP) is defined as ($SAR/H^2 \cdot f$), where H and f are the field and the frequency of the field, respectively. The maximal intrinsic loss power (ILP) was determined to be 9.6 nHm^2/kg, which is much higher than that reported in previous works[11,21] (Table III). This high ILP value once again confirms the good dispersion of magnetic particles in aqueous medium with the assistance of the PAA outer coating.

CONCLUSIONS

In this work, high-quality magnetic fluid was synthesized by thermal decomposition using poly(-acrylic acid) as phase transfer ligand. The additional organic coating layer improved the stability of the magnetic particles in aqueous solution. These highly stable magnetic particles also exhibited good magnetic heating induction. The highest temperature (70.22°C) was obtained for the sample concentration of 5 mg/ml when applying an alternative magnetic field with amplitude of 80 Oe and frequency of 178 kHz. These results appear promising for the application of nano-sized Fe_3O_4 fluid in hyperthermia cancer treatment and MRI.

ACKNOWLEDGEMENTS

This research was supported by DT.NCCB-DHUD.2012-G/08 of The National Foundation for Science and Technology Development (NAFOSTED) and funded in part by the AOSRD award FA 2386 14-1-0025.

REFERENCES

1. X. Meng, H.C. Seton, T. Lu Le, I.A. Prior, N.T. Thanh, and B. Song, *Nanoscale* 3, 977 (2011).
2. L.T. Lu, L.D. Tung, J. Long, D.G. Fernig, and N.T.K. Thanh, *J. Mater. Chem.* 19, 6023 (2009).
3. J.H. Lee, Y.M. Huh, Y.W. Jun, J.W. Seo, J.T. Jang, H.T. Song, S. Kim, E.J. Cho, H.G. Yoon, J.S. Suh, and J. Cheon, *Nat. Med.* 13, 95 (2007).
4. W.S. Seo, J.H. Lee, X. Sun, Y. Suzuki, D. Mann, Z. Liu, M. Terashima, P.C. Yang, M.V. McConnell, D.G. Nishimura, and H. Dai, *Nat. Mater.* 5, 971 (2006).
5. M. Gonzales-Weimuller, M. Zeisberger, and K.M. Krishnan, *J. Magn. Magn. Mater.* 321, 1947 (2009).
6. B. Mehdaoui, A. Meffre, J. Carrey, S. Lachaize, L.-M. Lacroix, M. Gougeon, B. Chaudret, and M. Respaud, *Adv. Funct. Mater.* 21, 4573 (2011).
7. P.L. Hariani, M. Faizal, R. Ridwan, M. Marsi, and D. Setiabudidaya, *Int. J. Environ. Sci. Dev.* 4, 336 (2013).
8. T.J. Daou, G. Pourroy, S. Begin-Colin, J.M. Greneche, C. Ulhaq-Bouillet, P. Legare, P. Bernhardt, C. Leuvrey, and G. Rogez, *Chem. Mater.* 18, 4399 (2006).
9. S. Sun, H. Zeng, D.B. Robinson, S. Raoux, P.M. Rice, S.X. Wang, and G. Li, *J. Am. Chem. Soc.* 126, 273 (2004).
10. D. Maity, S.-G. Choo, J. Yi, J. Ding, and J.M. Xue, *J. Magn. Magn. Mater.* 321, 1256 (2009).
11. T.K.O. Vuong, D.L. Tran, T.L. Le, D.V. Pham, H.N. Pham, T.H.L. Ngo, H.M. Do, and X.P. Nguyen, *Mater. Chem. Phys.* 163, 537 (2015).
12. D. Ling and T. Hyeon, *Small* 9, 1450 (2013).
13. H. Wei, N. Insin, J. Lee, H.-S. Han, J.M. Cordero, W. Liu, and M.G. Bawendi, *Nano Lett.* 12, 22 (2012).
14. J. Xie, C. Xu, N. Kohler, Y. Hou, and S. Sun, *Adv. Mater.* 19, 3163 (2007).
15. T. Zhang, J. Ge, Y. Hu, and Y. Yin, *Nano Lett.* 7, 3203 (2007).
16. D.K. Nagesha, B.D. Plouffe, M. Phan, L.H. Lewis, S. Sridhar, and S.K. Murthy, *Appl. Phys.* 105, 07B317 (2009).
17. Y. Xu, L. Zhuang, H. Lin, H. Shen, and J.W. Li, *Thin Solid Films* 544, 368 (2013).
18. X. Yaolin, Y. Qin, S. Palchoudhury, and Y. Bao, *Langmuir* 27, 8990 (2011).
19. L.L. Balcells, J. Fontcuberta, B. Martinez, and X. Obradors, *J. Phys. Condens. Matt.* 10, 1883 (1998).
20. T.T. Luong, T.P. Ha, L.D. Tran, M.H. Do, T.T. Mai, N.H. Pham, H.B.T. Phan, G.H.T. Pham, N.M.T. Hoang, Q.T. Nguyen, and P.X. Nguyen, *Colloid. Surf. A* 384, 23 (2011).
21. Y.V. Kolenko, M.B. Lopez, C. Rodriguez-Abreu, E. Carbo-Argibay, A. Sailsman, Y. Pineiro-Redondo, M.F. Cerqueira, D.M. Petrovykh, K. Kovnir, O.I. Lebedev, and J. Rivas, *J. Phys. Chem. C* 118, 8691 (2014).